Analytic modified embedded atom potentials for HCP metals

2001 J. Phys.: Condens. Matter 13 1193

(http://iopscience.iop.org/0953-8984/13/6/302)

INSTITUTE OF PHYSICS PUBLISHING JOURNAL OF PHYSICS: CONDENSED MATTER

J. Phys.: Condens. Matter **13** (2001) 1193–1213 www.iop.org/Journals/cm PII: S0953-8984(01)16793-7

Analytic modified embedded atom potentials for HCP metals

Wangyu Hu[1,2], **Bangwei Zhang**[1], **Baiyun Huang**[2], **Fei Gao**[3,4] **and David J Bacon**[3]

[1] College of Materials Science and Engineering, Hunan University, Changsha 410082, People's Republic of China
[2] Powder Metallurgy Research Institute, Central South University, Changsha 410083, People's Republic of China
[3] Materials Science and Engineering, Department of Engineering, University of Liverpool, Liverpool L69 3GH, UK
[4] Pacific Northwest National Laboratory, MS K-44, PO Box 999, Richland, WA 99352, USA

Received 4 September 2000, in final form 7 December 2000

Abstract

Analytic modified embedded atom method (AMEAM) type many-body potentials have been constructed for ten hcp metals: Be, Co, Hf, Mg, Re, Ru, Sc, Ti, Y and Zr. The potentials are parametrized using analytic functions and fitted to the cohesive energy, unrelaxed vacancy formation energy, five independent second-order elastic constants and two equilibrium conditions. Hence, each of the constructed potentials represents a stable hexagonal close-packed lattice with a particular non-ideal c/a ratio. In order to treat the metals with negative Cauchy pressure, a modified term has been added to the total energy. For all the metals considered, the hcp lattice is shown to be energetically most stable when compared with the fcc and bcc structure and the hcp lattice with ideal c/a. The activation energy for vacancy diffusion in these metals has been calculated. They agree well with experimental data available and those calculated by other authors for both monovacancy and divacancy mechanisms and the most possible diffusion paths are predicted. Stacking fault and surface energy have also been calculated and their values are lower than typical experimental data. Finally, the self-interstitial atom (SIA) formation energy and volume have been evaluated for eight possible sites. This calculation suggests that the basal split or crowdion is the most stable configuration for metals with a rather large deviation from the ideal c/a value and the non-basal dumbbell (C or S) is the most stable configuration for metals with c/a near ideal. The relationship between SIA formation energy and melting temperature roughly obeys a linear relation for most metals except Ru and Re.

1. Introduction

The application of computer simulation using empirical pair potential interactions between atoms has been less common for hcp metals than cubic metals because of the difficulty of obtaining suitable interatomic potentials [1, 2]. Furthermore, although the embedded atom

potentials (EAM) proposed by Daw and Baskes [3] and many-body potentials introduced by Finnis and Sinclair [4] (F–S) give a more realistic picture of crystal properties than can be obtained by pair potentials, there have been few studies using these kinds of potentials for the hcp metals (e.g. [5–9]). The most extensive sets derived to date are those of F–S type by Igarashi *et al* [7] and EAM type by Baskes and Johnson [9]. The potentials proposed by Igarashi *et al* for the eight metals Be, Hf, Ti, Ru, Zr, Co, Mg and Zn were fitted to several physical parameters, including the c/a ratio, but not to any data that arise from atom–atom interactions inside the normal equilibrium lattice spacing. This may be a rather serious problem for interstitial modelling because the perfect crystals defined by these potentials require a much higher hydrostatic pressure to produce a small volume decrease than is found experimentally. In other words, the pair repulsion term is very 'hard' and this can be expected to lead to values of interstitial atom formation energy that are too large. Moreover, Bacon found that some potentials produce an unstable crystal when used to model twin boundaries [2] and this must put their suitability for simulating point defects into question. The modified EAM potentials proposed by Baskes and Johnson [9] with angular forces were applied to 18 hcp metals. They studied the vacancy, divacancy, stacking fault and surface, but the divacancy was unbound in all of the metals considered except Be. Moreover, no information was given about the application of their model to self-interstitial atoms.

The EAM potentials proposed by Johnson *et al* [5, 10, 11] are short range and have the virtue of fitting the empirical energy–volume relationship of Rose *et al* [12], thereby ensuring reasonable response for atomic spacings inside the equilibrium spacing. In the first and third papers, potentials were derived for Mg, Ti and Zr, but all with the ideal c/a ratio (1.633). In the second paper, two 'model' potentials which approximately match zirconium were described, one with c/a close to the ideal value and the other with 1.580, which is below the real ratio of 1.593. Ackland [13, 14] has developed F–S potentials for Ti and Zr by fitting to three elastic constants and one lattice constant. These potentials also give a good description of atom–atom interactions inside the nearest-neighbour spacing and have been employed successfully to investigate defects, surface and displacement-threshold properties, radiation damage and twin boundary structures. Therefore, existing interatomic many-body potentials for atomic-scale simulation of hcp metals are only appropriate for metals such as Mg, Ti and Zr which have a c/a lattice parameter ratio close to the ideal value and new potentials are required for further study of a wide range of metals.

In the present study, new analytic modified EAM many-body potentials for hcp metals are developed. We construct these potentials to reproduce exactly the observed c/a ratio and all five elastic constants for each metal are considered. These potentials guarantee the stability of the hexagonal structure with respect to hcp with ideal c/a, fcc and bcc crystal structures. The formation and migration energies of the vacancy, the activation energy for self-diffusion of monovacancy, the divacancy formation and binding energies and the activation energy for diffusion by a divacancy mechanism are calculated and discussed. Finally, stacking fault and surface energies and the self-interstitial atom (SIA) formation energy for eight possible sites have been evaluated. In addition, the phonon spectra have been calculated and discussed in another paper. A good agreement between measured and calculated phonon spectra has been obtained for the acoustic branches and a reasonable agreement has been obtained for optical branches for all elements studied.

2. Form and construction of the potentials

In the original EAM model, there are two assumptions [3, 15]. First, the atomic electron densities are to be well represented by the spherically averaged free atom densities calculated

from Hartree–Fock theory by Clementi and Roetti [16] and McClean and McClean [17]. Second, the host electron density is approximated by a linear superposition of the atomic densities of the constituents. These assumptions are too simple and cannot describe the actual situation well. Baskes [18] modified the EAM to include directional bonding in the expression of electron density and applied it to silicon and recently extended it to a variety of cubic materials [19]. Pasianot *et al* [20] added a new term in the form of total energy for the EAM to represent a many-body shear term related to bond angles in a global (average) sense. Zhang *et al* [21, 22] modified Johnson's analytic EAM, in a similar way to Pasianot. They added a modified analytic energy term $M(P)$ to the total energy expression for the EAM to express the difference between the actual total energy of a system of atoms and that calculated from the original EAM using a linear superposition of spherical atomic electron densities. The model was successful for calculating the vacancy diffusion mechanism for all bcc transition metals [22] and the thermodynamic properties of their binary alloys [21]. A similar approach is now developed here for hcp metals.

The physical properties fitted within this scheme are the cohesive energy, E_c, unrelaxed vacancy formation energy, E_{1f}, five independent second-order elastic constants and the two lattice constants of the hexagonal structure, a and c. All these quantities are summarized in table 1.

Table 1. Quantities used in the fitting of the potentials. Values of a and c have been taken from Barrett and Massalski [23], values of E_c from Kittel [24] and vacancy formation energies from Baskes and Johnson [9]. Values of elastic constants of Be and Y are from Simmon and Wang [25], those of other elements from Brandes and Brook [26], only C_{33} of Be and Ru is modified for fitting from 336.4 to 246 and from 624 to 535, respectively. a and c are in nm, E_c and E_{1f} in eV and C_{ij} in GPa.

	a	c	E_c	E_{1f}	C_{11}	C_{12}	C_{44}	C_{13}	C_{33}
Be	0.228 56	0.358 32	3.32	1.11	292.3	26.7	162.5	14	246
Co	0.249 70	0.406 90	4.39	1.35	295	159	71	111	335
Hf	0.319 46	0.505 11	6.44	1.80	181	77	55.7	66	197
Mg	0.320 94	0.521 05	1.51	0.58	59.3	25.7	16.4	21.4	61.5
Re	0.276 00	0.445 80	8.03	2.30	616	273	161	206	683
Ru	0.270 57	0.428 16	6.74	1.85	563	188	181	168	535
Sc	0.330 80	0.526 70	3.90	1.15	99.3	39.7	27.2	29.4	107
Ti	0.295 06	0.467 88	4.85	1.50	160	90	46.5	66	181
Y	0.364 74	0.573 06	4.37	1.25	77.9	28.5	24.31	21.0	76.9
Zr	0.323 12	0.514 77	6.25	1.70	144	74	33.4	67	166

The basic equation of the total energy of a system of atoms is

$$E_t = \sum E_i \tag{1}$$

where the contribution from the atom at site i is

$$E_i = F(\rho_i) + \frac{1}{2}\sum \phi(r_{ij}) + M(P_i) \tag{2}$$

For simplification, we denote equation (2) as

$$E = F(\rho) + \frac{1}{2}\sum_m \phi(r_m) + M(P) \tag{3}$$

where m represents the mth-neighbour distance and the energy modification term is empirically taken as

$$M(P) = \alpha\left\{1 - \exp\left[-\left(\ln\left|\frac{P}{P_e}\right|\right)^2\right]\right\}. \tag{4}$$

The host electron density is taken in the original form

$$\rho = \sum_m f(r_m) \tag{5}$$

and the argument of the energy modification term P is taken as

$$P = \sum_m f^2(r_m) \frac{r_{mx}^2 + r_{my}^2 + \beta r_{mz}^2}{r_m^2} \tag{6}$$

where r_{mx}, r_{my} and r_{mz} represent the component of vector $\boldsymbol{r}_m$ connecting the atom m to the atom chosen as the origin and the coordinate system is chosen such that the z-axis is parallel to the c-axis of the hexagonal lattice and x- and y-axes are in the basal plane. If the considered atom is not in the origin, at any coordinate (x_0, y_0, z_0), the argument of the energy modification term P is taken as the general form

$$P = \sum_m f^2(r_m) \frac{(x_m - x_0)^2 + (y_m - y_0)^2 + \beta(z_m - z_0)^2}{(x_m - x_0)^2 + (y_m - y_0)^2 + \beta(z_m - z_0)^2} \tag{7}$$

where (x_m, y_m, z_m) is the coordinate of the surrounded atoms and r_m is the distance between the considered atom and its surrounded atom. Thus, the present potential can be applied in the problems where the orientation of crystalline axes is physically defined. For the case of grain or tilt boundaries, all atomic positions can be defined in a coordinate system, so the present potential can be applied. However, the present form of the potential is not invariant with respect to a chosen coordinate system. It should be improved in further work.

The energy modification term was first introduced to resolve the negative Cauchy pressure problem in Johnson's model and the argument P is presented as the sum of high orders of electron density in order to correct the discrepancy of the linear superposition of atomic electron density at the same time. Thus, the number of parameters in the modified term should be the same as the number of Cauchy relations for the specific crystal. In the cubic structure, there is only one Cauchy relation among the three elastic constants, so one parameter is enough to describe the Cauchy discrepancy. However, there are two Cauchy relations among the five elastic constants for an hcp crystal, so, we introduce two parameters in the modified term to interpret this anisotropy: one is α in equation (4) and the other β in the argument P as in equation (6). As described below, these two parameters can be determined from the equations describing the two Cauchy relations between C_{11} and C_{12} and between C_{13} and C_{44}.

The atomic density $f(r)$ and embedding function $F(\rho)$ take the same forms as those used by Johnson and Oh [10]:

$$f(r) = f_e \left(\frac{r_1}{r} \right)^6 \tag{8}$$

$$F(\rho) = -F_0 \left[1 - n \ln \left(\frac{\rho}{\rho_e} \right) \right] \left(\frac{\rho}{\rho_e} \right)^n \tag{9}$$

where $F_0 = E_c - E_{1f}$. f_e is taken as unity as was done by Johnson [10]. ρ_e and P_e take their equilibrium values. n is an adjustable parameter and its specific value for each element is determined by fitting the empirical energy–volume relationship of Rose *et al* [12], which ensures reasonable response for atomic spacing just inside the first-neighbour distance. To ensure the curves of the cohesive energy dependence on the c/a ratio continuity, the cut-off distance of atomic electron density should be larger than that of the potential. In the present model, potentials out to the seventh-neighbour distance are considered and truncated at a

specific cutoff distance $r_c = \frac{1}{4}(6a + \sqrt{a^2 + c^2})$. Thus, the atomic density $f(r)$ is truncated at a specific cutoff distance

$$r_{ce} = 2a + \frac{3}{4}\left(\sqrt{\frac{13}{3}a^2 + \frac{1}{4}c^2} - 2a\right).$$

If the distance is larger than r_{ce}, we let $f(r)$ be equal to zero.

The vacancy formation energy E_{1f} is the energy difference between a crystal with one vacancy lattice site and a perfect crystal containing the same number of atoms. In this formalism, this unrelaxed vacancy formation energy can be approximately represented with the pair potential approximation for fitting purposes [10], i.e.

$$E_{1f} = -\frac{1}{2}\sum_m \phi(r_m). \tag{10}$$

The conditions of equilibrium can be expressed as a requirement that there are no stresses in the perfect crystal. Stresses, σ_{ij}, in a system of particles can be evaluated by expanding the energy to the first order with respect to an infinitesimal homogeneous strain applied to the system [27, 28]. In the present case this leads to

$$\Omega_0\sigma_{ij} = \frac{1}{2}\sum_m \frac{r_{mi}r_{mj}}{r_m}\phi'(r_m) \tag{11}$$

where r_{mi} is the ith component of the vector $\boldsymbol{r}_m$ connecting the atom m to the atom chosen as the origin and Ω_0 is the equilibrium atomic volume. With the coordinate system chosen as described above, it follows from symmetry that $\sigma_{xx} = \sigma_{yy}$ and $\sigma_{xy} = \sigma_{xz} = \sigma_{yz} = 0$. The equilibrium conditions which have to be satisfied for given value of a and c are then

$$\sigma_{xx} = 0 \qquad \sigma_{zz} = 0. \tag{12}$$

The second-order elastic constants, C_{ijkl}, can be evaluated by expanding the energy of the system to the second order with respect to an infinitesimal homogeneous strain [27], and are composed of two terms for the hcp lattice. One relates to the strain which is homogeneous everywhere in the system while the second arises due to the possible relative displacements of different sublattices when a macroscopic homogeneous strain is applied. The latter term, named inner elastic constants, was analysed in detail by Martin [29], who has also shown that the relaxation of sublattices contributes only to the second order and does not therefore affect the stresses. When fitting the elastic constants, the second term is neglected as done by Johnson [30, 10] and Igarashi *et al* [7]. Hence the following formulae have been used when fitting the elastic constants:

$$\begin{aligned}\Omega_0 C_{ijkl} = {} & F''(\rho)\sum_m \frac{r_{mi}r_{mj}}{r_m}f'(r_m)\sum_m \frac{r_{mk}r_{ml}}{r_m}f'(r_m) \\ & + \frac{1}{2}\sum_m \frac{r_{mi}r_{mj}r_{mk}r_{ml}}{r_m}\left[\phi''(r_m) - \frac{\phi'(r_m)}{r_m}\right] \\ & + 4M''(P)\sum_m \frac{r_{mi}}{r_m^2}f^2(r_m)\left(r_{mx}\delta_{xj} + r_{my}\delta_{yj} + \beta r_{mz}\delta_{zj} - 7r_{mj}\frac{r_{mx}^2 + r_{my}^2 + \beta r_{mz}^2}{r_m^2}\right) \\ & \times \sum_m \frac{r_{mk}}{r_m^2}f^2(r_m)\left(r_{mx}\delta_{xl} + r_{my}\delta_{yl} + \beta r_{mz}\delta_{zl} - 7r_{ml}\frac{r_{mx}^2 + r_{my}^2 + \beta r_{mz}^2}{r_m^2}\right).\end{aligned} \tag{13}$$

Hence, with the five equations for the elastic constants (including the two Cauchy relations in them) and the two equations of equilibrium and one equation for the vacancy formation energy, there are eight equations for fitting for an hcp crystal.

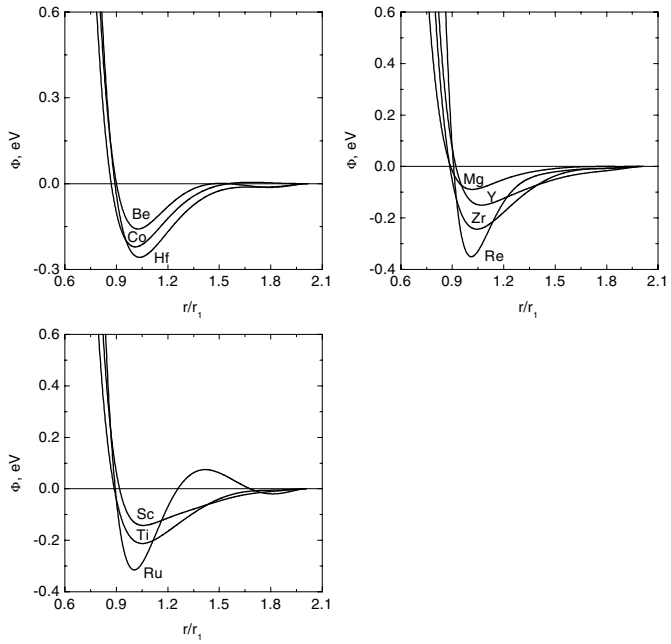

Figure 1. Potentials for hcp metals.

The next step is to choose the effective pair potential function. In the present model, atomic interactions out to the seventh neighbour distance are considered and $\phi(r)$ are truncated at a specific cutoff distance $r_c = \frac{1}{4}(6a + \sqrt{a^2 + c^2})$. At this point, the pair potential and its slope are zero, i.e.

$$\phi(r_c) = 0 \tag{14}$$

$$\phi'(r_c) = 0 \tag{15}$$

and so two parameters should be added to the pair potential function for this cutoff procedure. We take this potential function as

$$\phi(r) = \sum_{j=-1}^{j=6} k_j \left(\frac{r}{r_1}\right)^j \tag{16}$$

and so with the three equations for the elastic constants in the pair potential scheme, the two equations of equilibrium, the equation for the vacancy formation energy and the two equations of the cutoff procedure, the eight model parameters k_j ($j = -1, 0, 1, 2, 3, 4, 5, 6$) in the potential function can be resolved analytically.

Using the data for a and c, E_c, unrelaxed vacancy formation energy E_{1f} and C_{11}, C_{12}, C_{44}, C_{33} and C_{13} from table 1 as the input parameters, all 12 model parameters n, F_0, α, β, k_j can be determined with the above equations and the Rose equation [12]. The model parameters calculated in this way are listed in table 2.

All of the pair potentials and embedding functions for these metals are shown in figure 1 and figure 2, respectively. A distinct minimum near the nearest-neighbour distance can be seen. The modified functions are shown in figure 3. The modification term can be positive or negative, depending on the two Cauchy relations of elements, i.e. it is negative for metals with negative Cauchy pressure, such as Be, Mg, Ru, Sc and Y. Thus, there is no difficulty in describing elements with negative Cauchy pressure with the present model.

Table 2. Parameters of the many-body potentials for hcp metals. n is dimensionless, F_0, α, β and k_i are in eV.

	Be	Co	Hf	Mg	Re	Ru	Sc	Ti	Y	Zr
n	0.98	0.58	0.32	0.75	0.48	0.58	0.70	0.48	0.60	0.53
F_0	2.21	3.04	4.64	0.93	5.73	4.89	2.75	3.35	3.12	4.55
α	−0.4798	0.01422	0.01656	−0.0384	0.04182	−0.2294	−0.1473	0.03005	−0.1496	0.00604
β	1.00490	−1.2182	−0.9289	3.76607	−0.9303	1.21617	1.76217	−0.9450	1.93961	−1.0284
k_{-1}	154.410	123.185	196.078	103.569	803.604	257.768	278.060	169.887	227.685	159.684
k_0	−699.29	−541.74	−897.48	−480.43	−3777.7	−1094.2	−1327.2	−806.22	−1078.0	−737.50
k_1	1352.79	1009.10	1758.20	945.667	7520.87	1958.03	2692.65	1637.53	2175.94	1459.80
k_2	−1457.1	−1038.2	−1918.9	−1026.4	−8243.2	−1933.9	−3011.7	−1847.0	−2429.2	−1610.1
k_3	946.627	639.281	1261.61	664.156	5360.53	1150.51	2005.28	1247.62	1619.29	1068.40
k_4	−371.30	−235.94	−499.29	−256.28	−2076.7	−416.33	−794.62	−503.61	−644.08	−425.73
k_5	81.3505	48.3404	109.947	54.6063	443.583	85.4510	173.495	112.266	141.461	94.1193
k_6	−7.6651	−4.2398	−10.371	−4.9557	−40.317	−7.6976	−16.101	−10.646	−13.228	−8.8869

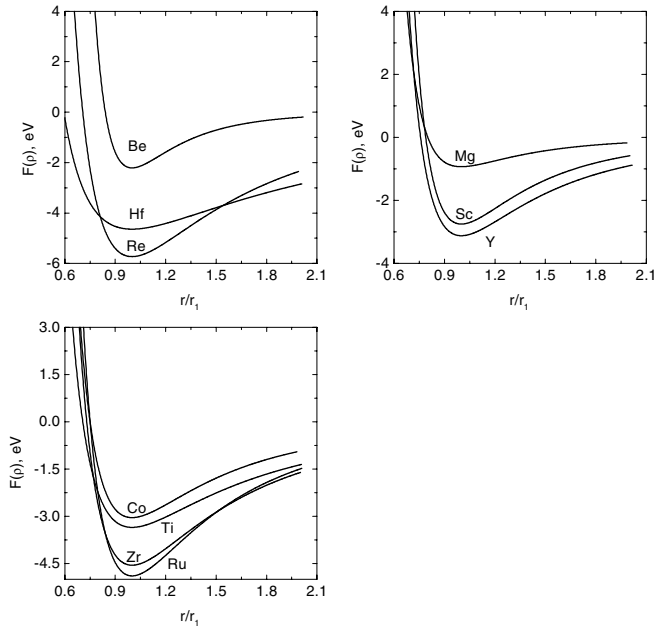

Figure 2. Embedding functions for hcp metals.

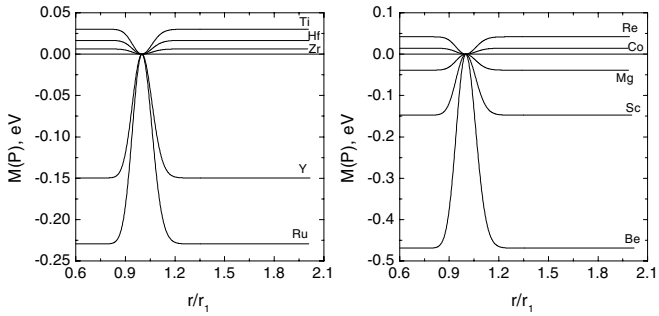

Figure 3. Modified functions for hcp metals.

Rose *et al* [12] obtained a universal equation of energy versus volume empirically for a broad range of materials. To ensure reasonable behaviour for atom–atom interactions inside the equilibrium spacing, this empirical relationship was fitted inside the first-neighbour distance by adjusting parameter n. Figure 4 shows the comparison of the curve of total energy for the present model with that from the Rose equation. Since the five elastic constants are input parameters, the elastic constants calculated with the present model are fitted exactly, except for C_{33} of Be and Ru. For these two metals, attempts to fit the potentials with the experimental data of C_{33} were unsuccessful due to problems of mechanical and structural stability.

3. Tests and applications of the potentials

3.1. Mechanical and structural stability

Since the potentials constructed here are intended for use in atomistic simulations of crystal defects, they must ensure that no unphysical structural instabilities occur, not only for small

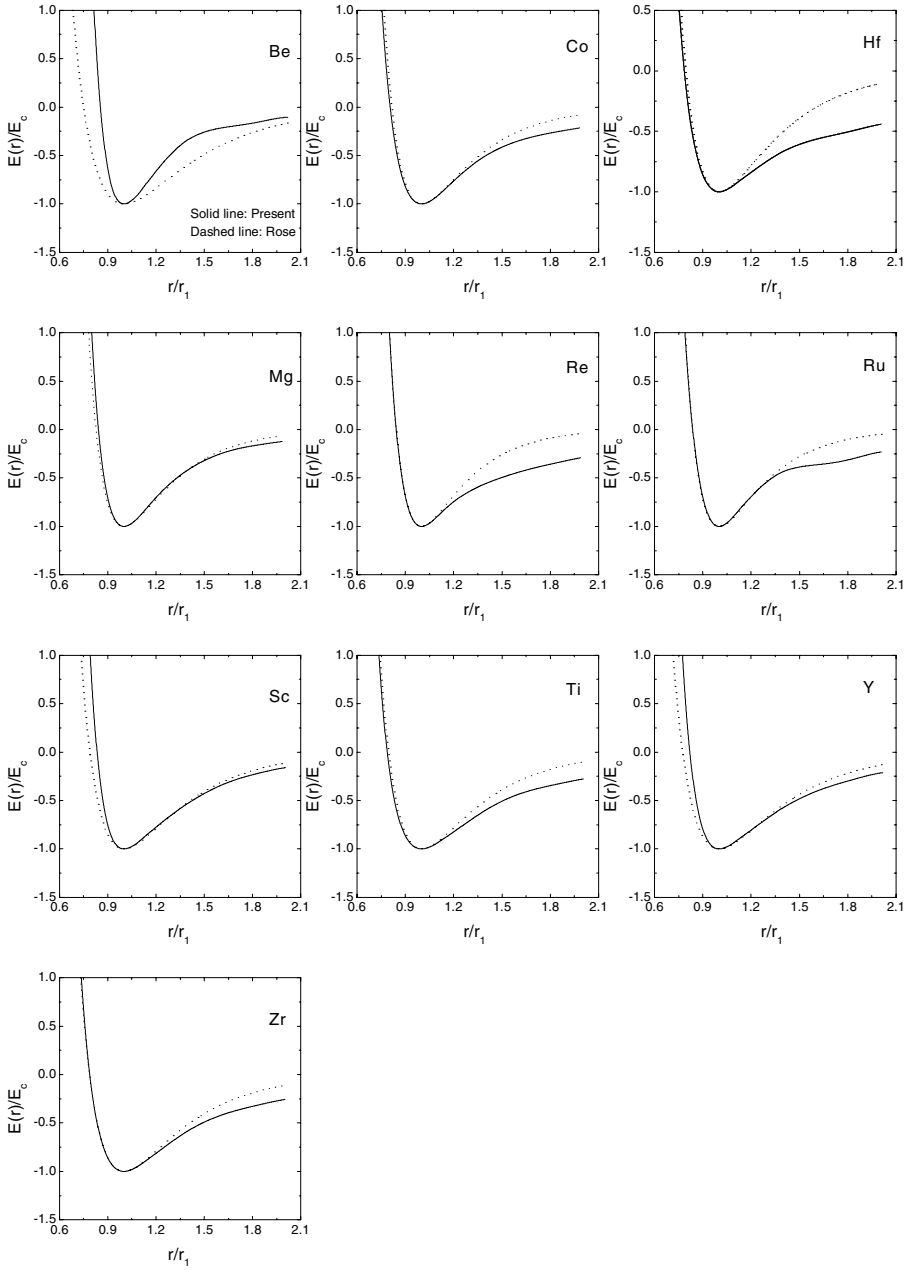

Figure 4. The total energies as a function of r/r_1 for hcp metals. The solid curves are the results calculated from the present model; the dashed curves are the results from the Rose equation.

but for large deformations. Furthermore, it is necessary that the potentials do not favour other lattice structures over the hcp crystal they represent. The lattice stability is calculated here under the assumption of constant volume, which is the same as was done by Johnson and Oh [10] and Zhang *et al* [22] for the bcc metals. In table 3, the lattice stability (in eV per atom) relative to the hcp structure with ideal c/a ratio is predicted. The structural energy difference

Table 3. Calculated and experimental values of lattice stabilities for hcp with ideal c/a ratio, fcc and bcc crystal structures relative to the real hcp structure (in eV/atom).

	Hcp (ideal c/a)		Fcc				Bcc		
	Present	Baskes [9]	Present	Baskes [9]	Pasianot [8]	Exp. [31]	Present	Baskes [9]	Exp. [31]
Be	0.0086	0.0077	0.0060	0.057		0.063	0.0310	0.074	0.068
Co	0.0000	0.0000	0.0062	0.005	0.007		0.0164	0.241	
Hf	0.0068	0.0059	0.0068	0.053	0.039	0.100	0.0301	0.064 0.059	
Mg	0.0001	0.0000	0.0022	0.004	0.0083	0.026	0.0176	0.029	0.031
Re	0.0018	0.0005	0.0050	0.031		0.110	0.1636	0.303	0.292
Ru	0.0117	0.0124	0.0003	0.114		0.125	0.0755	0.268	0.265
Sc	0.0025	0.0016	0.0010	0.023			0.0501	0.248	
Ti	0.0041	0.0071	0.0094	0.033	0.023	0.060	0.0143	0.075 0.070	
Y	0.0059	0.0075	0.0017	0.052			0.0440	0.300	
Zr	0.0029	0.0105	0.0049	0.017		0.076	0.0179	0.061	0.076

is near zero for metals with a near-ideal c/a ratio, such as Co and Mg. It increases rapidly with decreasing c/a ratio. These relaxation energies range up to 0.01 eV. Figure 5 shows the relation between the structural energy difference $(E_{hcp,\ ideal\ c/a} - E_{hcp})/E_c$ and $(1.633 - c/a)$ for the metals considered. The solid circles represent the present calculations and the dashed line is the fitting result with a second-order polynomial function for these points. The squares are the calculated results of Baskes and Johnson [9]. From this figure, it can be seen that the structural energy difference increases nonlinearly with the difference between ideal c/a and real c/a. This implies that the approximation of the real hcp structure to the ideal c/a hcp structure is reasonable only for metals with a near-ideal c/a ratio. Metals with a much smaller or larger c/a than this must be treated according to their real structures. The structural stability of the close-packed hexagonal lattice relative to fcc and bcc is also shown in table 3. It is seen that the fitted hcp lattice is indeed the most stable one, although the energy difference is rather small for fcc compared with experimental data [31] and those of others [8, 9]. Agreement with experiment [31] and Baskes' data [9] for bcc is fair.

The mechanical stability of the hcp lattice with respect to large homogeneous expansions and compressions (in general not pure hydrostatic) has been tested for each potential. This was done by calculating the energy of the hcp crystal for different values of the atomic volume, Ω and c/a ratio. Figure 6 shows the dependence of cohesive energy on c/a at different values of Ω for Hf. It is seen that in this range of the c/a values and volume changes, no other hcp metastable configurations exist under the constructed potential. Moreover, the c/a ratio corresponding to the lowest energy structure increases with decreasing Ω, that is with increasing compression and converges towards the ideal value, 1.633. Clearly, under high compression the atoms tend to behave like hard spheres owing to strong repulsion. The same results have been found for all the potentials constructed.

3.2. Surface and stacking fault energy

The defect and surface calculations were carried out using the molecular dynamics code MOLDY [32]. They were simulated in parallelepiped blocks of up to 4860 atoms at constant pressure with periodic boundary conditions.

In general, the dominant feature of the surface is the relaxation of the atoms so as to optimize their effective coordination and in particular an inward relaxation of the upper layer is predicted with many-body potentials, in contrast to the direction obtained with pair poten-

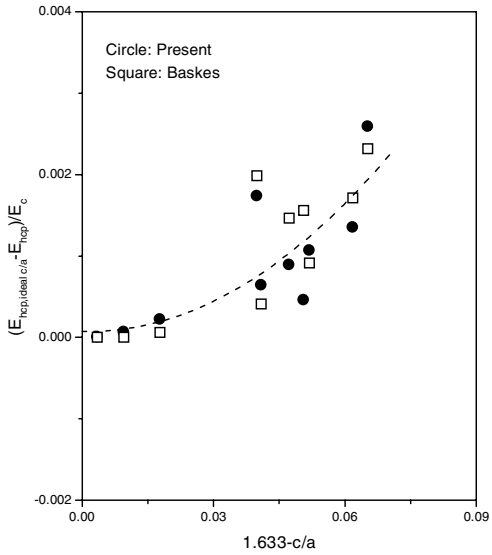

Figure 5. Relation between the structural energy difference $(E_{hcp,\ ideal\ c/a} - E_{hcp})/E_c$ and $(1.633 - c/a)$.

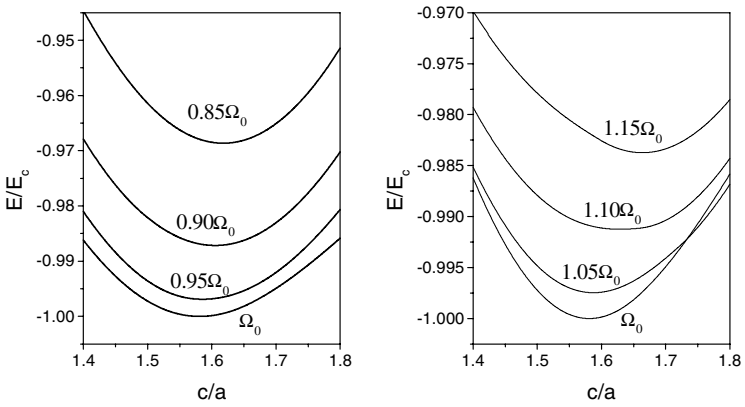

Figure 6. Dependence of cohesive energy on c/a ratio at different values of the atomic volume for Hf.

tials. The surface energy is ordered with crystallographic orientation as one would expect from bond-breaking considerations, but the variation is not as great as arguments based on bond-breaking would suggest. The surface energy has been calculated following the methodology of Ackland [13] and the results are summarized in table 4. The calculated surface energies for the basal and prism planes are about equal, both are less than the experiments (average surface extrapolated to 0 K), except for the case of Be and Sc where the calculated energy is somewhat higher. The agreement with experiment for the present calculations is worse compared with the results of Baskes and Johnson [9] and it is close to the results for Ti [13] and Zr [14] with F–S many-body potentials.

There has been considerable speculation over the years about the possible existence of stacking faults in the hcp metals, particularly in relation to dislocation glide and loop-habit

Table 4. Calculated and experimental values of surface energy (mJ m^{-2}).

	Basal plane		Prism plane		
Element	Present	Others	Present	Others	Experimental data
Be	1273	1650 [9]	1294	795 [9]	1150 [33]
Co	1162	3056 [9]	1172	3454 [9]	2550 [34], 2160 [33]
Hf	992	2041 [9]	988	1636 [9]	2150 [34], 2190 [33]
Mg	310	900 [9]	316	1016 [9]	785 [33]
Re	1682	3940 [9]	1689	3949 [9]	3600 [34], 3630 [33]
Ru	1281	3191 [9]	1308	1994 [9]	3050 [34], 3040 [33]
Sc	706	1355 [9]	706	1295 [9]	410 [33]
Ti	1033	1962 [9], 993 [13]	1023	1673 [9], 1039 [13]	2100 [34], 1920 [33]
Y	623	1001 [9]	626	738 [9]	1125 [33]
Zr	988	2302 [9], 1022 [14]	978	2364 [9], 1230 [14]	2000 [34], 2050 [33]

planes. Possible stacking faults in hcp metals were enumerated by Bacon and Liang [35] and stacking fault energy was calculated by them using a variety of pair potentials. There are three possible faults on the basal plane, whose energies are loosely incorporated in the fitting procedure via the fcc–hcp energy difference. The two intrinsic faults have one of the two stacking sequences ABABCBCB (I_1) and ABABCACA (I_2), whilst the extrinsic fault has the stacking sequence ABABCABAB (E). The most important fault is the I_2 type intrinsic stacking fault, so most of the reported values of stacking fault energy are for this. A relatively wide dislocation splitting has been observed in Co and its stacking fault energy is estimated to be 27 mJ m^{-2} [36]. The only experimental estimate for Ti [37] is of the order of 300 mJ m^{-2}. The stacking fault energy in all hexagonal metals was calculated by Legrand using the pseudopotential approach for divalent elements and a tight-binding method for transition elements [38]. These calculations suggest very high stacking fault energies for all the transition metals as well as for Be but energies of the order of 30–40 mJ m^{-2} for Mg, Co and Zn.

In the framework of the many-body potentials constructed in this paper the stacking fault energy is principally determined by the values of embedding functions and the pair potentials for atomic separations at and beyond seventh neighbours. Using the constructed potentials, the stacking fault energies I2, I1 and E have been calculated and are summarized in table 5. Reasonable stacking fault energies have been obtained for Co and Mg. However, the calculated stacking fault energies in the other metals are much lower than those reported by others [7, 9, 14, 36–38]. Attempts to adjust the potentials so as to achieve a higher stacking fault energy were unsuccessful due to problems of lattice stability.

3.3. Vacancy and divacancy

Using the present model, it is possible to calculate the formation and migration energies of the vacancy, the sum of which is the activation energy for self-diffusion by the vacancy mechanism and the divacancy. The relaxed vacancy formation energy and formation volume have been calculated with MOLDY and are listed in table 6. (The unrelaxed vacancy formation energy E_{1f} (equation (6)) is shown in brackets.) The difference of the vacancy formation energy between relaxed and unrelaxed values is small, not more than 0.05 eV. The migration energy for a vacancy is the difference between the energy for an atom at the saddle point and that at its equilibrium site as it moves from its crystal site to the nearest vacant site. For hcp metals, there are two saddle points in this path, denoted as C and B_c respectively, which correspond to the migration of an atom out of the basal plane and in the basal plane. The

Table 5. Calculated and experimental values of the unrelaxed stacking fault energies (mJ m^{-2}).

Element	I_2	I_1	E	I_2 reported by others
Be	102	51	153	414 [9], 390 [38], 357 [7]
Co	37	18	55	30 [9], 42 [38], 27 [36], 64 [7]
Hf	45	22	67	198 [9], 390 [38], 111 [7]
Mg	8	4	12	14 [9], 30 [38], 10 [7]
Re	31	16	44	150 [9], 540 [38]
Ru	68	34	119	588 [9], 875 [38], 213 [7],397 [7]
Sc	12	6	18	78 [9]
Ti	47	24	71	144 [9], 290 [38], 300 [37],116 [7]
	64 [13]	33 [13]	94 [13]	
Y	21	10	31	148 [9], 210 [38]
Zr	26	13	40	62 [9], 340 [38], 27 [7]
	80 [14]	41 [14]	118 [14]	

present calculations for the migration energies E_{1m}^{out} and E_{1m}^{in} and then the activation energy for self-diffusion $Q_{1v}^{out} = E_{1m}^{out} + E_{1f}$ (out of plane) and $Q_{1v}^{in} = E_{1m}^{in} + E_{1f}$ (in plane) are also shown in table 6. The experimental data and the data predicted or cited are also included: they focus on the metals with c/a ratio close to ideal, such as Co, Mg, Zr and Ti. The agreement between the present calculations and those data from experiment or other authors is rather good for the formation, migration and activation energies. It should be pointed out that diffusion activation energies from [40] are calculated with the Engel–Brewer theory and do not consider the specific diffusion path and the results are much higher than the experimental data. The present results are better than those obtained by Johnson and Beeler [46], Liu *et al* [43] and others.

It is interesting to compare the out-of-basal plane and in-basal plane self-diffusion energy. Bacon [1, 2] reviewed these data obtained before 1993. Using different pair potentials, the isotropic nature of vacancy migration is observed for Ti and Co and the migration in the basal plane is preferred for Mg; however, the out-of-plane migration is preferred for Zr [1]. Another paper reported that the migration in the basal plane was slightly preferred for Zr [52]. Using the many-body potential of Ti, the migration energy of the in-plane and the out-of-plane mechanisms is 0.80 and 0.68 eV, respectively [2]. Oh and Johnson found the activation energy for self-diffusion in Zr to be independent of a change in the c/a ratio and the migration in the basal plane was preferred [50]. Because the available data are limited and contradictory, a systematic study is necessary. The present study reveals that Q_{1v}^{in} is equal to or larger than Q_{1v}^{out}, so the diffusion in the non-basal plane is easier than that in the basal plane. Moreover, our calculations indicate that the c/a ratio strongly affects the microdiffusion mechanism. The isotropic nature of vacancy migration is observed for Mg and Co whose c/a ratio is close to the ideal value and the migration in the out-of-plane is preferred for other metals. The experimental data of the diffusion activation energy of Be are 1.708 and 1.631 eV/atom for basal and non-basal plane, respectively [39]; this implies that the migration in the out-of-plane is preferred. The present calculations are agreement with these experimental data.

Diffusion is dominated by the contribution of mono-vacancies, but the contribution of di-vacancies may be significant at high temperature and so we have considered it with the new potentials. The self-diffusion activation energy is the sum of the formation and migration energies of a divacancy, but diffusion in hcp metals is different from that in fcc and bcc metals due to the different positions of near-neighbour sites. We therefore investigate the divacancy formation and binding energies for several possible divacancy structures and found the first-

Table 6. Predicted and experimental monovacancy properties.

Metals	Value	Present work (eV)	Experimental data (eV)	Data by others (eV)	Formation volume (Ω_0)		c/a
					Present	Others	
Be	E_{1f}	1.12 (1.13)	1.11 [9]	1.23 [9]	0.97		1.568
	E_{1m}^{out}	0.62					
	Q_{1v}^{out}	1.74 (1.75)	1.631 [39]				
	E_{1m}^{in}	0.64					
	Q_{1v}^{in}	1.76 (1.77)	1.708 [39]	2.420 [40]			
Co	E_{1f}	1.38 (1.40)	1.35 [9]	1.41 [41], 1.48 [9]	0.78	1.630	
	E_{1m}^{out}	0.72		0.89 [41]			
	Q_{1v}^{out}	2.10 (2.12)		2.301 [41]			
	E_{1m}^{in}	0.72		0.89 [41]			
	Q_{1v}^{in}	2.10 (2.12)		2.30 [41]			
Hf	E_{1f}	1.80 (1.82)	1.80 [9]	2.02 [9]	0.95		1.581
	E_{1m}^{out}	0.90					
	Q_{1v}^{out}	2.70 (2.72)					
	E_{1m}^{in}	0.98					
	Q_{1v}^{in}	2.78 (2.80)					
Mg	E_{1f}	0.59 (0.59)	0.58 [9], 0.87 [42]	0.66 [9], 0.87 [43]	0.83		1.624
	E_{1m}^{out}	0.35	0.39 [43],	0.66 [42]			
	Q_{1v}^{out}	0.94 (0.94)	1.388 [44]	1.26 [43], 1.43 [40, 45],	1.45 [42]		
	E_{1m}^{in}	0.35		0.40 [43], 0.59 [42]			
	Q_{1v}^{in}	0.94 (0.94)		1.27 [43], 1.38 [42], 1.44 [45]			
Re	E_{1f}	2.35 (2.36)	2.30 [9]	2.49 [9]	0.89		1.615
	E_{1m}^{out}	2.25					
	Q_{1v}^{out}	4.60 (4.61)					
	E_{1m}^{in}	2.29					
	Q_{1v}^{in}	4.64 (4.65)					
Ru	E_{1f}	1.87 (1.88)	1.85 [9]		2.11 [9]	0.94	1.582
	E_{1m}^{out}	1.79					
	Q_{1}^{out}	3.66 (3.67)					
	E_{1m}^{in}	1.87					
	Q_{1v}^{in}	3.74 (3.75)					
Sc	E_{1f}	1.14 (1.18)	1.15 [9]		1.28 [9]	0.79	1.592
	E_{1m}^{out}	0.57					
	Q_{1v}^{out}	1.71 (1.75)					
	E_{1m}^{in}	0.59					
	Q_{1v}^{in}	1.73 (1.77)					
Ti	E_{1f}	1.49 (1.54)	1.50 [9]	1.49 [11,46], 1.80 [9], 1.43 [13]	0.76	0.80 [13]	1.586
	E_{1m}^{out}	0.56		0.82 [11], 0.68 [2], 1.28 [46]			
	Q_{1v}^{out}	2.05 (2.10)	1.272 [47]	2.31 [11], 2.77 [46], 3.014 [40]			
	E_{1m}^{in}	0.61		0.67 [11], 0.80 [2], 1.28 [46]			
	Q_{1v}^{in}	2.10 (2.15)		2.16 [11], 2.77 [46]			
Y	E_{1f}	1.22 (1.27)	1.25 [9]	1.39 [9]	0.93		1.571
	E_{1m}^{out}	0.55					
	Q_{1v}^{out}	1.77 (1.82)	1.336 [48]	2.791 [40]			
	E_{1m}^{in}	0.59					
	Q_{1v}^{in}	1.81 (1.86)					
Zr	E_{1f}	1.70 (1.75)	1.70 [9]	1.55 [49], 1.93 [9], 1.86 [50]	0.80	0.74 [14]	1.593
	E_{1m}^{out}	0.67		0.785 [50], 1.07 [49]			
	Q_{1v}^{out}	2.37 (2.42)		2.645 [50], 2.62 [49]			
	E_{1m}^{in}	0.72		0.775 [50], 1.18 [49]			
	Q_{1v}^{in}	2.42 (2.47)	1.975 [51]	2.635 [50], 2.73 [49], 3.296 [40]			

nearest neighbours (FN) and the second-nearest neighbours (SN) to be much more stable than other configurations and so only these two need be considered. The results are listed in table 7. (The data in brackets are unrelaxed values.) The formation energy of a divacancy in the non-basal plane is almost the same as that in the basal plane in all metals and the relaxed values are almost the same as the unrelaxed ones, the maximum difference being only 0.03 eV. Results calculated by other authors are also included in this table. The model proposed by Baskes and Johnson [9] can only predict the binding of divacancy for Be, because it is negative for other metals. Comparing the results of other authors with those obtained here, it can be seen that they are somewhat different in magnitude, but all give positive binding energy, which indicates that these configurations are stable.

Table 7. Calculated divacancy formation and binding energies (in eV/atom).

	FN (out of plane)			SN (in plane)		
Metals	Formation energy (eV)	Binding energy (eV)	Formation volume (Ω_0)	Formation energy (eV)	Binding energy (eV)	Formation volume (Ω_0)
Be	2.11 (2.13)	0.13 (0.13) 0.21 [9]	1.99	2.09 (2.12)	0.15 (0.15) 0.17 [9]	1.98
Co	2.56 (2.59)	0.20 (0.20) 0.400 [41]	1.57	2.57 (2.61)	0.19 (0.19) 0.440 [41]	1.59
Hf	3.35 (3.41)	0.24 (0.24)	1.90	3.35 (3.41)	0.24 (0.24)	1.90
Mg	1.10 (1.11)	0.08 (0.08) 0.131 [1]	1.66	1.09 (1.10)	0.09 (0.09) 0.133 [1]	1.67
Re	4.38 (4.40)	0.32 (0.32)	1.79	4.40 (4.42)	0.32 (0.31)	1.80
Ru	3.46 (3.48)	0.28 (0.29)	1.90	3.45 (3.48)	0.29 (0.28)	1.88
Sc	2.17 (2.25)	0.11 (0.11)	1.60	2.15 (2.24)	0.13 (0.12)	1.60
Ti	2.78 (2.89) 2.58 [39] 2.76 [11]	0.20 (0.19) 0.40 [46] 0.22 [11]	1.47	2.79 (2.90) 2.36 [39] 2.76 [11]	0.20 (0.18) 0.62 [46] 0.22 [11]	1.51
Y	2.32 (2.43)	0.12 (0.12)	1.86	2.29 (2.42)	0.15 (0.13)	1.86
Zr	3.18 (3.29)	0.21 (0.21) 0.236 [50] 0.08 [52]	1.60	3.18 (3.29)	0.22 (0.21) 0.248 [50] 0.10 [52]	1.60

For the migration of a divacancy in hcp metals, two configurations (FN and SN) should be considered. Figure 7 shows the possible diffusion paths in these configurations. The results are shown in table 8. It can be seen that the difference of diffusion activation energies between these configurations is not large and the divacancy migration energy depends slightly on the migration path. The smallest migration energy for FN is almost the same as for SN. In the case of FN, j_1 and j_2 paths may be the most probable diffusion path due to the lowest activation energies. After migration of atoms along the j_1 path, the divacancy retains the FN configuration, so continuous migration can proceed. After migration of atoms along the j_1 path, the divacancy retains the FN configuration, so continuous migration can proceed. After migration of atoms along the j_2 path, the divacancy transfers to the SN configuration, so continuous migration can proceed with FN or SN configuration. In the case of SN, the j_1 and j_2 paths are the most probable and after migration of an atom along the j_2 path, the configuration of the SN divacancy is retained; in a similar way, after migration of an atom along the j_1 path, the configuration of the SN divacancy transfers to FN. There is little in the literature about the diffusion of the divacancy in hcp metals. Johnson [11, 46] studied it for Ti and Mikhin *et al* studied it for Zr [52]: their data are in agreement with our results.

Table 8. Divacancy migration and diffusion activation energies (in eV/atom).

		Be	Co	Hf	Mg	Re	Ru	Sc	Ti	Y	Zr
E_{j1}^{FN}		0.60	0.59	0.75	0.29	1.83	1.63	0.45	0.43	0.44	0.54
E_{j2}^{FN}		0.61	0.61	0.74	0.30	1.86	1.63	0.45	0.43	0.43	0.53
E_{j3}^{FN}		0.70	0.79	1.07	0.37	2.39	2.00	0.63	0.68	0.63	0.80
E_{j4}^{FN}		0.64	0.77	0.96	0.37	2.29	1.81	0.61	0.62	0.59	0.74
E_{j5}^{FN}		0.64	0.75	1.02	0.36	2.31	1.83	0.63	0.66	0.59	0.77
E_{j6}^{FN}		0.61	0.73	0.92	0.36	2.26	1.75	0.60	0.58	0.58	0.70
Q_{2v}^{FN}	min.	2.71	3.15	4.09	1.39	6.21	5.09	2.62	3.21	2.75	3.71
	max.	2.81	3.35	4.42	1.47	6.77	5.46	2.80	3.46	2.95	3.98
									3.15 [40]		3.12 [52]
									3.40 [17]		3.74 [52]
E_{j1}^{SN}		0.62	0.59	0.75	0.29	1.82	1.64	0.45	0.43	0.45	0.53
E_{j2}^{SN}		0.62	0.58	0.81	0.28	1.88	1.71	0.47	0.46	0.47	0.58
E_{j3}^{SN}		0.67	0.80	0.99	0.38	2.35	1.91	0.60	0.62	0.59	0.75
E_{j4}^{SN}		0.62	0.75	0.94	0.37	2.27	1.75	0.60	0.60	0.58	0.72
E_{j5}^{SN}		0.63	0.75	1.01	0.36	2.31	1.82	0.63	0.66	0.62	0.77
E_{j6}^{SN}		0.63	0.72	0.99	0.35	2.30	1.84	0.61	0.63	0.61	0.74
Q_{2v}^{SN}	min.	2.71	3.15	4.10	1.37	6.22	5.09	2.60	3.22	2.74	3.71
	max.	2.76	3.37	4.36	1.47	6.65	5.36	2.78	3.45	2.91	3.95
									2.88 [40]		3.44 [52]
									3.28 [17]		

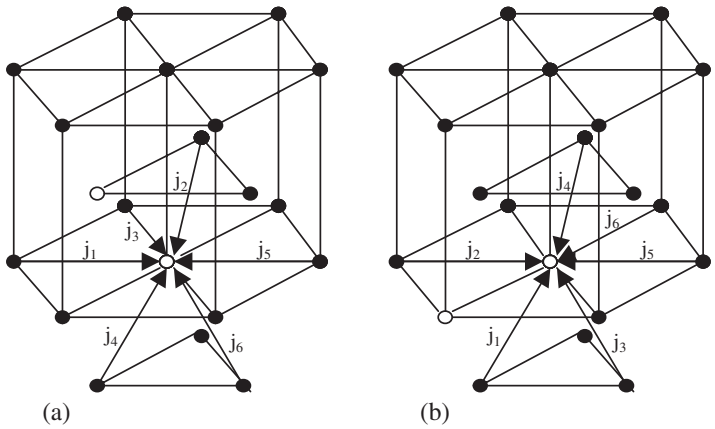

Figure 7. The divacancy diffusion mechanism for hcp metals with c/a less than ideal: (a) FN; (b) SN.

3.4. Self-interstitial atoms

Self-interstitial atom (SIA) formation energy and volume have been calculated for eight sites that have been suggested as possible interstitial positions [46]. An O site is centred in an octahedron, a T site in a tetrahedron, a C site (crowdion) is midway between two out-of-plane nearest neighbours and an S site is a split (dumbbell) configuration normal to the basal plane. Similarly, for interstitials in the basal plane, a B_O site is below an O site, a B_T site is below a T site, a B_C site is a crowdion midway between two in-plane nearest neighbours and a B_S site is a split (dumbbell) configuration in the basal plane.

The formation energy and volume are listed in table 9, where the initial site and relaxed configuration are also shown. Note that several configurations are unstable and transform to a stable one. There is only one stable interstitial position (Bs) for Be, all other SIAs transform to Bs after relaxation. For the SIAs in the basal plane, Bt transforms to Bs or Bc. Bo is stable for Co, Hf, Mg, Ru, Ti, Y and Zr; it transforms to Bc for Re and Sc. Bc is stable for all metals except Be. Bs is stable for all metals. The SIAs in the non-basal plane are general stable for all metals except Be, but O transforms to Bc for Hf, O transforms to Bo and T to Bs for Ru and T transforms to Bc for Sc. The most stable SIA is Bs for Be and Ru, is Bs or Bc for Hf, Sc, Y and Zr and is non-basal dumbbell for other metals. Thus, the basal split or crowdion is the most stable configuration for metals with a rather large deviation from the ideal c/a value and the non-basal dumbbell (C or S) is the most stable configuration for metals with c/a near ideal. However, Igarashi *et al* [7] reported that the pyramidal plane crowdion was most stable for all eight metals (Be, Hf, Ti, Ru, Zr, Co, Mg, Zn) and Bacon [2] gave a general preference for the basal octahedral site with pair potential calculations for Co, Ti and Zr, which is somewhat in contrast with the present work. These results are in agreement with those of Johnson [5, 11, 46] for Ti and Ackland *et al* [14] for Zr. As pointed out by Ackland [13], the non-ideal c/a ratio is important in stabilizing the basal crowdion, since the basal 'nearest neighbours' are slightly farther apart than those in adjacent planes. Moreover, the c/a ratio affects the relaxed configuration of SIA greatly.

Different potentials have yielded different results for SIA formation energy. The dominant effects in determining formation energy are the repulsion (which determines how much the surrounding atoms are pushed away) and the elastic constants, which describe how the energy of the strain field around the interstitial is taken up. Bacon [1] reviewed the simulation results for SIA of hcp metals published until 1993. He found the formation energy was predicted to lie in the range $\sim$14–36kT_m, where k is Boltzmann's constant and T_m is melting temperature. Moreover, he suggested that the reasonable value of formation energy of SIA should fall in the range of 18–25kT_m from the calculations with the pair and many-body potentials. The lowest formation energy of SIA for these metals is plotted against kT_m in figure 8. The formation energy increases linearly as melting temperature increases for most metals except Ru and Re. This gives a rough relationship between SIA formation energy and kT_m, i.e. $E_{if} = 19kT_m$. Because the present potentials give a good description of all five elastic constants and the appropriate energy–volume relationship for small volume changes, the present values of SIA formation energy should be reasonable. They are in fair agreement with that of Ackland for Ti [13] and Ackland *et al* [14] for Zr. It should be noted that, while the absolute value of the interstitial formation energy is very sensitive to the hardness of the potential core, the relative energies depend more on the crystal structure and elastic constants. Hence the large discrepancy between the current values and those obtained with the similar potentials of Igarashi *et al* [7] (hard core) and Oh and Johnson [5] (large C_{66}) can be explained.

The potentials presented here have a long range and are of an equilibrium nature, in contrast with the short-range F–S potentials which have been widely employed to simulate defect properties in metals. The long-range potentials have certainly some advantages in representing certain properties of metals in comparison with short-range potentials. Osetsky *et al* [53] employed a long-range pair interatomic potential (LRPP) and a short-range potential (MBP) of Finnis–Sinclair type to simulate the structure and properties of vacancy loops and stacking-fault tetrahedral (SFT) in copper. The results show that the short-range equilibrium potential is not favourable for planar vacancy platelet to collapse into either loops or tetrahedra. It seems that the collapsed structures (tetrahedra) are stable with the MBPs, but the potentials cannot provide a relaxation path to them. A similar qualitative result was obtained by Shimomura *et al* [54] using an equilibrium EAM potential with a range up to the third-nearest neighbour.

Table 9. Calculated formation energies and volumes for self-interstitial atom at different positions.

Elements	Initial site	Relaxed configuration	Formation energy (eV)		Formation volume (Ω_0)	
			Present	Others	Present	Others
Be	C	Bs	2.96	10.5 [7]	0.90	
	B_O	Bs	2.96	11.63 [7]	0.90	
	B_C	Bs	2.96	11.51 [7]	0.90	
	B_T	Bs	2.96	11.60 [7]	0.90	
	B_S	Bs	2.96		0.90	
	O	Bs	2.96	11.51 [7]	0.90	
	S	Bs	2.96	11.66 [7]	0.90	
	T	Bs	2.96	11.67 [7]	0.90	
Co	C	Dumb	3.48	23.9 [7]	0.78	
	B_S	Bs	3.54		0.75	
	S	Dumb	3.53	25.03 [7]	0.77	
	B_C	B_C	3.48	24.97 [7]	0.78	
	B_T	B_C	3.48	25.14 [7]	0.78	
	O	Dumb	3.48	24.93 [7]	0.78	
	T	Dumb	3.48	25.08 [7]	0.78	
	B_O	B_O	3.62	25.01 [7]	0.72	
Hf	C	Dumb	4.73	9.5 [7]	0.68	
	B_C	B_C	4.64	10.52 [7]	0.59	
	B_S	Bs	4.64		0.59	
	O	B_C	4.64	10.52 [7]	0.59	
	S	Dumb	5.18	10.67 [7]	0.75	
	T	Dumb	4.73	10.67 [7]	0.68	
	B_O	B_O	4.72	10.64 [7]	0.59	
	B_T	Bs	4.64	10.63 [7]	0.59	
Mg	C	Dumb	1.76	2.02 [5], 7.1 [7]	1.16	
	B_S	Bs	1.80		1.10	
	O	Dumb	1.76	2.08 [5], 8.12 [7]	1.16	
	S	Dumb	1.76	2.19 [5], 8.24 [7]	1.16	
	B_C	B_C	1.80	8.16 [7]	1.08	
	B_T	Bs	1.80	8.30 [7]	1.10	
	T	Dumb	1.76	8.30 [7]	1.16	
	B_O	B_O	1.86	2.12 [5], 8.27 [7]	1.06	
Re	C	Dumb	11.90		1.45	
	B_S	Bs	11.98		1.37	
	B_C	B_C	11.99		1.38	
	B_T	B_C	11.99		1.38	
	S	Dumb	11.90		1.45	
	T	Dumb	11.90		1.45	
	B_O	Bc	11.98		1.38	
	O	Dumb	11.90		1.45	
Ru	C	Dumb	9.06	27.3 [7]	0.73	
	B_S	Bs	8.70		0.63	
	O	Bo	8.79	28.31 [7]	0.60	
	S	Dumb	9.02	28.45 [7]	0.73	
	B_C	B_C	8.71	28.34 [7]	0.64	
	B_T	Bs	8.70	28.46 [7]	0.63	
	T	Bs	8.70	28.45 [7]	0.63	
	B_O	B_O	8.79	28.45 [7]	0.60	
Sc	C	Dumb	3.31		1.28	
	B_S	Bs	3.29		1.19	
	S	Dumb	3.31		1.28	

Table 9. (Continued)

Elements	Initial site	Relaxed configuration	Formation energy (eV)		Formation volume (Ω_0)	
			Present	Others	Present	Others
	B_C	B_C	3.29		1.19	
	B_O	B_C	3.29		1.19	
	B_T	B_C	3.29		1.19	
	T	Dumb	3.31		1.28	
	O	Dumb	3.31		1.28	
Ti	C	Dumb	2.92	3.82 [11], 3.76 [5], 3.07 [13], 7.7 [7]	0.76	1.18 [11], 0.96 [13]
	B_S	Bs	2.95	3.85 [11]	0.60	1.50 [11]
	B_C	B_C	2.96	3.70 [11], 8.75 [7]	0.60	1.25 [11]
	B_T	B_C	2.96	3.45 [11], 8.87 [7]	0.60	1.11 [11]
	O	Dumb	2.92	3.45 [11], 3.86 [5], 8.77 [7]	0.76	1.23 [11]
	T	Dumb	2.92	3.39 [11], 8.86 [7]	0.76	1.36 [11]
	B_O	B_O	3.07	3.33 [11], 3.79 [5], 8.88 [7]	0.60	1.18 [11]
	S	Dumb	3.15	4.05 [11], 4.04 [5], 8.86 [7]	0.78	1.26 [11]
Y	C	Dumb	3.28		0.97	
	B_S	Bs	3.23		0.88	
	S	Dumb	3.28		0.98	
	B_C	B_C	3.23		0.85	
	B_T	Bs	3.23		0.88	
	T	Dumb	3.23		0.85	
	B_O	B_O	3.36		0.92	
	O	Dumb	3.32		1.04	
Zr	C	Dumb	3.60	4.52 [5], 3.65 [52], 3.979 [14], 7.7 [7]	0.69	0.27 [14]
	B_S	Bs	3.51	3.49 [52], 3.760 [14]	0.60	0.35 [14]
	B_O	B_O	3.58	3.46 [52], 3.970 [14], 8.90 [7]	0.61	0.30 [14]
	B_C	B_C	3.52	3.756 [14], 8.75 [7]	0.60	0.33 [14]
	B_T	Bs	3.51	8.84 [7]	0.60	
	O	Dumb	3.57	8.68 [7]	0.67	
	S	Dumb	3.57	3.85 [52], 4.319 [14], 8.83 [7]	0.67	0.20 [14]
	T	Dumb	3.57	8.88 [7]	0.67	

They found that a vacancy cluster was relaxed close to a SFT, but a clear picture of a SFT was not presented. It would be of interest to use the present potentials to study defect clusters in hcp metals, particularly for vacancy clusters and to compare with those obtained by the short-range many-body potentials.

4. Conclusions

In this paper we have constructed EAM-type many-body potentials for ten hexagonal close-packed metals. These potentials reproduce for each metal considered the experimentally observed equilibrium density, c/a ratio, cohesive energy, five independent second-order elastic constants and, approximately, the vacancy formation energy. A modification term is introduced for describing metals with negative Cauchy pressure. To ensure the applicability of the potentials in the modelling of extended lattice defects, the mechanical stability of the corresponding hcp lattice with respect to large changes of density and c/a ratio was examined. At the same time the structural stability of the real hexagonal close-packed lattice relative to fcc, bcc and simple hexagonal structures was also tested. These tests all show that the fitted hcp lattice are the most stable structures. Four applications of the potentials, which at the

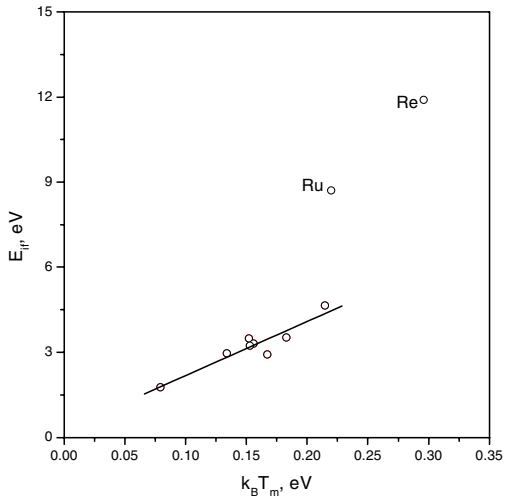

Figure 8. Relation between self-interstitial atom formation energy and melting temperature.

same time also represent tests, have been presented here. They are calculations of stacking fault energy, surface energy and study of possible vacancy and interstitial configurations. The calculated surface energies are reasonable, but the calculated stacking fault energies for most of elements are rather low. The activation energies for self-diffusion by mono-vacancies and di-vacancies are calculated and these results agree well with experimental data available and those calculated by other authors. Furthermore, the most favourable diffusion paths are predicted. Finally, the self-interstitial atom has several stable configurations. In general, the Bs or Bc is the most stable configuration for metals with a rather large deviation from the ideal c/a value and the non-basal dumbbell (C or S) is the most stable configuration for metals with c/a near ideal. The SIA formation energy is roughly proportion to the melting temperature for most metals except Ru and Re and it gives $E_{if} = 19kT_m$.

Acknowledgment

W Hu thanks Professor Pettifor and Dr Yu N Osetsky for their encouragement and helpful advice and is grateful for the award of a fellowship through the Royal Society of London for an extended visit to The University of Liverpool. This research was supported by the 'Trans-Century Training Programme Foundation for the Talents' and the 'Key Teacher Project' of the Minister of Education of China.

References

[1] Bacon D J 1988 *J. Nucl. Mater.* **159** 176
[2] Bacon D J 1993 *J. Nucl. Mater.* **249** 206
[3] Daw M S and Baskes M I 1984 *Phys. Rev.* B **29** 6443
[4] Finnis M W and Sinclair J E 1984 *Phil. Mag.* A **50** 45
[5] Oh D J and Johnson R A 1988 *J. Mater. Res.* **3** 471
[6] Willaime F and Massobrio C 1991 *Phys. Rev.* B **43** 11 653
[7] Igarashi M, Khantha K and Vitek V 1991 *Phil. Mag.* B **63** 603
[8] Pasianot R and Savino E J 1992 *Phys. Rev.* B **45** 12 704
[9] Baskes M I and Johnson R A 1994 *Modelling Simul. Mater. Sci. Eng.* **2** 147

[10] Johnson R A and Oh D J 1989 *J. Mater. Res.* **4** 1195
[11] Johnson R A 1991 *Phil. Mag.* A **63** 865
[12] Rose J H, Smith J R, Guinea F and Ferrante J 1984 *Phys. Rev.* B **29** 2963
[13] Ackland G J 1992 *Phil. Mag.* A **66** 917
[14] Ackland G J, Wooding S J and Bacon D J 1995 *Phil. Mag.* A **71** 553
[15] Johnson R A 1988 *Phys. Rev.* B **37** 3924
[16] Clementi E and Roetti C 1974 *At. Data Nucl. Data Tables* **14** 177
[17] McClean A D and McClean R S 1981 *At. Data Nucl. Data Tables* **26** 197
[18] Baskes M I 1987 *Phys. Rev. Lett.* **59** 2666
[19] Baskes M I 1992 *Phys. Rev.* B **46** 2727
[20] Pasianot R, Farkas D and Savino E J 1991 *Phys. Rev.* B **43** 6952
[21] Ouyang Y, Zhang B, Liao S and Jin Z 1996 *Z. Phys.* B **101** 161
[22] Zhang B, Ouyang Y, Liao S and Jin Z 1999 *Physica* B **262** 218
[23] Barrett C S and Massalski T B 1980 *Structure of Metals* 3rd edn (Oxford: Pergamon) p 626
[24] Kittel C 1976 *Introduction to Solid State Physics* (New York: Wiley) p 74
[25] Simmon G and Wang H 1971 *Single Crystal Elastic Constants and Calculated Aggregate Properties: a Handbook* (Cambridge, MA: MIT Press)
[26] Brandes E A and Brook G B (eds) 1992 *Smithells Metal Reference Book* 7th edn (Oxford: Butterworths) pp 15–16
[27] Born M and Huang K 1954 *Dynamical Theory of Crystal Lattices* (Oxford: Clarendon)
[28] Vitek V and Egami T 1987 *Phys. Status Solidi* b **144** 145
[29] Martin J W 1975 *J. Phys. C: Solid State Phys.* **8** 2858
[30] Johnson R A 1972 *Phys. Rev.* B **6** 2094
[31] Saunders N, Miodownik A P and Dinsdale A T 1988 *CALPHAD* **12** 351
[32] Ackland G J 1987 *DPhil Thesis* University of Oxford
[33] Tyson W R and Miller W A 1977 *Surf. Sci.* **62** 267
[34] de Boer F R, Boom R, Mattens M C M, Miedema A R and Nissen A K 1988 *Cohesion in Metals: Transition Metal Alloys* (Amsterdam: North-Holland)
[35] Bacon D J and M. H. Liang, *Phil. Mag.* A **53** 163
[36] Korner A and Karnthaler H P *Phil. Mag.* A **48** 469
[37] Partridge P G 1967 *Metall. Rev.* **12** 169
[38] Legrand P B 1984 *Phil. Mag.* B **49** 171
[39] Adda Y and Philibert J 1966 *La Diffusion Dans les Solides* vol II (Paris: Presses Universitaires De France) p 1132
[40] Cahoon J R and Sherby O D 1992 *Metall. Trans.* A **23** 2491
[41] Beeler J R Jr and Beeler M F 1981 *Interatomic Potentials and Crystalline Defects* ed J K Lee (New York: The Metallurgical Society AIME) p 141
[42] Bisio P H and Monti A M 1986 *Phys. Status Solidi* b **135** 545
[43] Liu X, Adams J B, Ercolessi F and Moriarty J A 1996 *Modelling Simul. Mater. Sci. Eng.* **4** 293
[44] Shewmon P G and Rhines F N 1954 *Trans. TMS-AIME* **200** 1021
[45] Combronde J and Brebec G 1971 *Acta Metall.* **19** 1393
[46] Johnson R A and Beeler J R Jr 1981 *Interatomic Potentials and Crystalline Defects* ed J K Lee (New York: The Metallurgical Society AIME) p 165
[47] Libanati C M and Dyment S F 1963 *Acta Metall.* **11** 1263
[48] Maskalets V N, Smimov E A, Skorov D M and Fedorov G B 1969 *Diffusion Data* **3** 35
[49] Fuse M 1985 *J. Nucl. Mater.* **136** 250
[50] Oh D J and Johnson R A 1989 *J. Nucl. Mater.* **169** 5
[51] Mrowec S 1980 *Defects and Diffusion in Solids—an Introduction (Materials Science Monographs 5)* (New York: Elsevier) p 396
[52] Mikhin A G, Osetsky Yu N and Kapinos V G 1994 *Phil. Mag.* A **70** 25
[53] Osetsky Yu N, Serra A, Victoria M, Golubov S I and Priego V 1999 *Phil. Mag.* A **79** 2259
[54] Shimomura Y, Mukouda I and Sugio K 1997 *J. Nucl. Mater.* **251** 61